KSCE Journal of Civil Engineering (2021) 25(12):4575-4584
DOI 10.1007/s12205-021-1623-3

pISSN 1226-7988, eISSN 1976-3808
www.springer.com/12205

Geotechnical Engineering

Seismic Rotational Stability Analysis of Gravity Retaining Wall under Heavy Rainfall

Xiaoguang Li[a] **and Jie Liu**[a]

[a]*School of Civil Engineering, Hebei University of Engineering, Handan 056000, China*

ARTICLE HISTORY

Received 22 September 2020
Revised 21 February 2021
Accepted 18 June 2021
Published Online 28 July 2021

KEYWORDS

Earthquake
Limit analysis
Heavy rainfall
Rotational stability
Seepage
Gravity retaining wall

ABSTRACT

A new methodology for the rotational stability analysis of a gravity retaining wall supporting inclined backfill under earthquake and heavy rainfall conditions has been presented. According to the movement mode of retaining wall and the characteristics of backfill sliding and rainwater infiltration, a sliding model of the infinite soil strip and rainwater infiltration model were established respectively. By calculating the internal energy dissipation rate and external loads power of the wall-soil system mechanism, a formula to calculate seismic yield acceleration coefficient under coupling conditions of earthquakes and rainfall was deduced. The results revealed a large effect size of infiltration depth of rainwater and the backfill inclination on the seismic yield acceleration coefficient. When the rainwater reaches 1/5 the height of the retaining wall and the backfill inclination exceeds 15°, the seismic yield acceleration coefficient will decrease rapidly. Moreover, the results obtained in this paper showed good consistency with those obtained by numerical simulation.

1. Introduction

The importance of the retaining wall is enormous and the design of these retaining structures is an important research topic for engineers. Gravity retaining walls are widely used in Geotechnical engineering for their simple form and convenient construction. For example, in a relatively mountainous area, people usually build the gravity retaining wall at the foot of mountains to prevent landslides. Earthquakes are also an important factor in causing landslides. Therefore, the seismic design of a gravity retaining wall becomes a key problem, especially in earthquake-prone areas. Some scholars paid attention to calculating earth pressure in seismic design, and many new methods have been developed. The most classical ones were presented by (Okabe, 1924) and Mononobe and Matsuo (1929). This method is still used by some scholars and some scholars have extended the method to make it more widely applicable. For example, Wilson and Elgamal (2015) and Jo et al. (2017) respectively used centrifugal experiments and shaking table experiments to determine the dynamic earth pressure on the retaining wall under seismic conditions and compared the results with the M-O method. The results showed that the displacement mode of the retaining wall has a great influence on the distribution and magnitude of the dynamic earth pressure. Leshchinsky et al. (2012) extended the M-O method to also apply to unstable slopes. However, the M-O method presents a basic shortcoming: the solution is based on the limit equilibrium of soil wedge without taking the retaining wall into account. So, Drucker et al. (1952) proposed the concept and theory of limit analysis, which was further developed by Chen and Liu (1990). The limit analysis includes the upper and lower bound theorems, and the upper bound theorem is an effective method to solve the limit state problem and has been widely used to solve the retaining wall problems.

In recent years, the multi-block theory has been widely used in Geotechnical engineering by some scholars. The application of multi-block analysis can improve the accuracy of the calculation model and make the model more in line with the actual situation. Li et al. (2015) investigated the sliding stability of the gravity retaining wall by dividing the backfill and the retaining wall into two wedges. Song et al. (2019) studied the seismic performance of earth slopes by establishing a series of rigid soil blocks parallel to the sliding surface. Pain et al. (2017) studied the seismic rotational stability of the retaining wall by solving the earth pressure generated by the entire soil wedge

CORRESPONDENCE Jie Liu jieliucqu@cqu.edu.cn School of Civil Engineering, Hebei University of Engineering, Handan 056000, China

behind the wall. Huang and Liu (2016) investigated the seismic rotational stability of the retaining wall by dividing the soil wedge into countless rigid soil slices parallel to the slip surface and establishing a kinematically admissible failure mechanism of the wall-soil system. But all of them are based on the dry state of the backfill. For the convenience of calculation, some scholars assumed the retaining wall with horizontal backfill surfaces when calculating the stability of the retaining wall. In fact, it has some restrictions on actual engineering. Chakraborty and Choudhury (2014a) and Li et al. (2010) found that the backfill inclination has a significant effect on the stability of the retaining wall. Similarly, the existence of water has a great impact on the stability of civil engineering buildings. Zhang et al. (2016), Chakraborty and Choudhury (2014a), Chakraborty and Choudhury (2014b), and Ahmad and Choudhury (2010) respectively studied the impact of water on retaining structures through different methods. The results indicated that the stability of the retaining structures was closely related to the saturated content of the soil. Chakraborty and Choudhury (2014a), Chakraborty and Choudhury (2014b), and Ahmad and Choudhury (2010) found that the soils were mostly saturated in the waterfront area, while Zhang et al. (2016) found the soils surrounding the foundation pits were commonly unsaturated. Rain is very common weather, rainwater that seeps into the soil can provide water for plants, but it can also damage the retaining structure. Every year, heavy rainfall can cause many natural disasters and engineering accidents. In the first half of 2020, there were many landslides caused by rainfall, which caused great economic losses to the Chinese people. Chandrasekaran et al. (2013) found that rainfall will cause landslides, retaining wall instability, and roadbed damage. Augusto Filho and Fernandes (2019) and Bo et al. (2019) investigated the impact of rainfall on landslides through field measurements and finite element analysis, respectively. The results showed that rainfall reduces soil self-stability by increasing soil weight and reducing soil cohesion. Rainwater infiltration is a very complicated process and it has always been a research hotspot. Yeh et al. (2020), Capparelli et al. (2020), and Zhang et al. (2014) discussed the influence of rainfall infiltration on slope stability. And some scholars established a series of rainwater infiltration models through experimental analysis, such as Xie-esaki-CAI model (Xie et al., 2004), Green-Ampt model (Green and Ampt, 1911), Lverson model (Iverson, 2000). Most of them believed that a sharp wetted front exists. Among them, the Green-Ampt model is widely used because of its convenience and simplicity. Green-Ampt model (Green and Ampt, 1911) supposed that the soil is fully saturated from the surface to the depth of the wetting front, while the soil below the wetting front is at the initial degree of saturation. Although many scholars have studied the effect of rainfall on the slope, a few have studied the effect of rainfall on the retaining walls. Retaining walls not only prevents some shallow landslides but also can reduce the permanent displacement of soil slopes after rainfall. Ren et al. (2020) used experimental methods to study the performance of reinforced retaining wall under earthquake and rainfall conditions. However, in some mountainous areas, gravity retaining wall is still a common retaining structure. Therefore, the influence of rainfall on the gravity retaining wall is worth discussing.

The upper bound method of limit analysis is an effective method to solve the limit state problem and has been widely used to solve the retaining wall problem. This paper attempted to derive a calculation method for the rotational seismic stability of a gravity retaining wall under rainstorm conditions. Firstly, this paper established the rainwater infiltration model and analyzed the loads on the wall-soil system. Then the failure mechanism of the wall-soil system was established by dividing the failure zone into numerous rigid soil strips parallel to the failure surface. An equivalent substitution model was used to calculate the water pressure of the rigid soil strip. Then, the seismic yield acceleration coefficient was deduced by calculating the internal energy dissipation and the work done by external loads. Finally, the influences of rainwater infiltration depth, backfill inclination, and wall-soil friction angle on seismic yield acceleration coefficient were investigated.

2. Theoretical Method

For the research of this paper, the following assumptions are made for the failure mode of rotating retaining walls in a cohesionless soil site. 1) The backfill is isotropic, homogeneous, cohesionless and has the same permeability coefficient (the hydraulic conductivity $k >> 10^{-3}$ cm/sec); 2) a sharp wetted front exists and the soil below the wetting front is in a dry state, while the soil above the wetting front is completely saturated; 3) the retaining wall is rigid and impermeable; 4) the retaining wall rotates only around the toe of the wall (point O in Fig. 1); 5) rainwater that does not seep into the backfill in time would flow

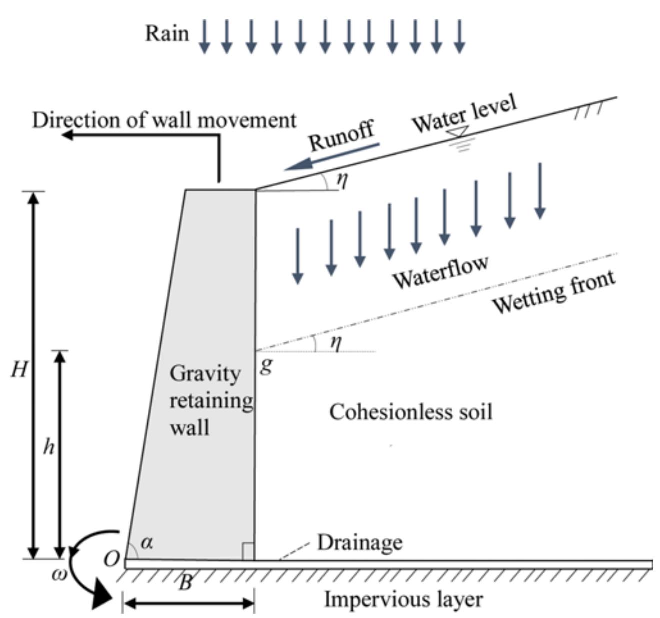

Fig. 1. Rainfall Infiltration Model of a Gravity Retaining Wall with Cohesionless Soil

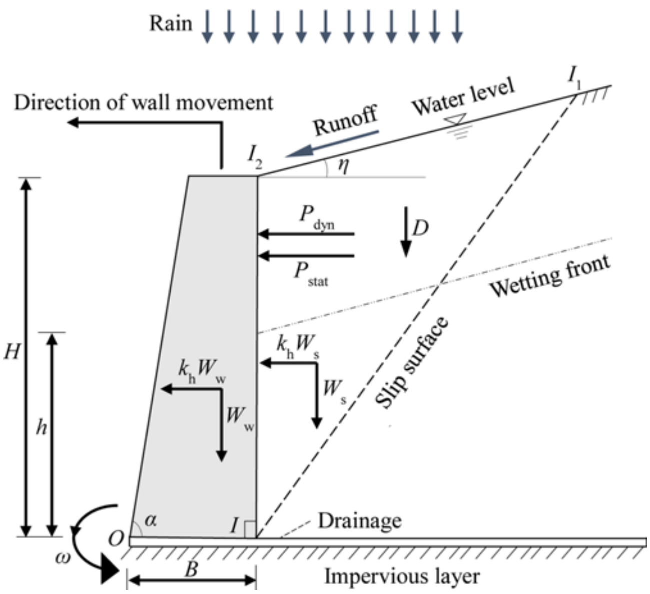

Fig. 2. Pure Rotates Failure Mechanism of a Gravity Retaining Wall

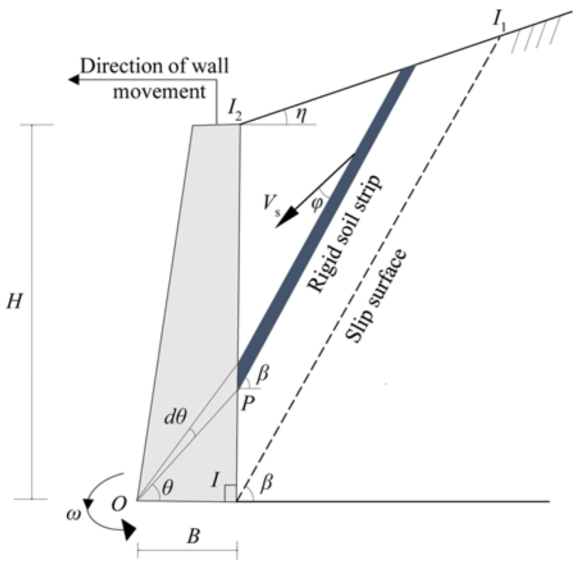

Fig. 3. An Infinite Number of Rigid Soil Strips

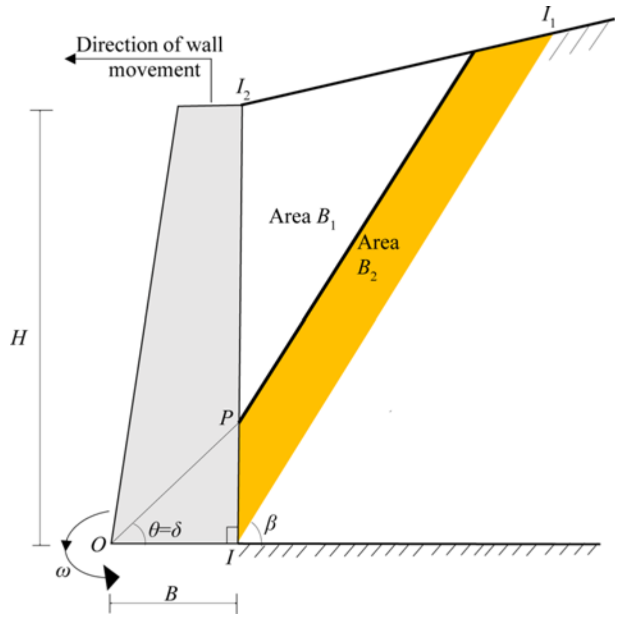

Fig. 4. Different Areas of Motion in the Velocity Field

along the backfill surface and would not accumulate on the ground; 6) runoff does not occur in the backfill during infiltration.

Figure 1 shows a gravity retaining wall with height H, width B, and the wall front inclination α. Due to rainfall, rainwater will infiltrate into the backfill and an obvious wetting front will appear in the backfill. And the infiltration depth will gradually increase as the rainfall time increases. If the rainwater reaches the base, excess water will run off from the drainage. In the upper bound theorem framework, the wall and soil wedge II_1I_2. (do not contain water) are treated as a wall-soil system. When the rate of work done by external loads exceeds the dissipation of internal loads, the wall will rotate about the wall toe (point O), and the wall top away from the backfill, and the backfill will slide downward. Note that due to the rotation mode of the wall, sliding speed of backfill will is not always the same.

Figure 2 shows that slip surface II_1 of a soil wedge II_1I_2 passes through the wall heel at an inclination angle β form horizontal. The wall-soil system is subjected to different loads due to rainfall and earthquake. In addition to gravity and horizontal seismic loads, the wall back is subjected to hydrostatic pressure (P_{stat}) and hydrodynamic pressure (P_{dyn}), while the backfill is subjected to water pressure.

2.1 Model Analysis

Figure 3 shows the soil wedge II_1I_2 is divided into numerous rigid soil strips parallel to the rupture surface II_1, and each rigid soil strip can be considered as a rectangle. So, the area of a rigid soil strip can be expressed by

$$dA_1 = \left(H - B\tan\theta\right)\cos\beta\frac{\sin(90^\circ+\eta)}{\sin\beta-\eta}dB\tan\theta$$
$$B\sec^2\theta\left(H - B\tan\theta\right)\cos\beta\frac{\cos\eta}{\sin\beta-\eta}d\theta. \tag{1}$$

2.2 Velocity Field Analysis

Zeng and Steedman (2000) put forward a calculation method for seismic earth pressure. When the retaining wall rotates around the toe of the wall, the backfill in area B_1 is in an active state and the backfill in area B_2 is in a passive state (in Fig. 4). As the retaining wall rotates, the velocity vector relationship between the P point and the adjacent rigid soil strip can be seen in Figs. 5 and 6. V_p and V_s are the velocities of the point P and the adjacent rigid soil strip, respectively, V_{ps} is the relative velocity between V_p and V_s, and the direction of V_{ps} is inclined at the angle δ from the wall-soil interface. Every point P on the wall has the same angular velocity as it rotates around the toe of the wall (point O). So, we can get

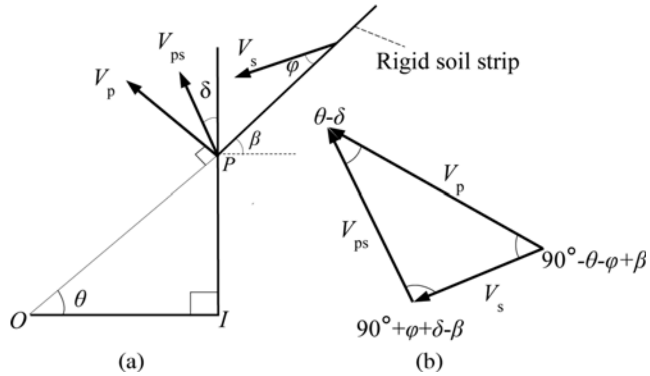

Fig. 5. Relative and Absolute Velocity Vectors for Case $\theta > \delta$: (a) Instantaneous Velocity of Point P and Adjacent Soil Strips, (b) Velocity Vector Triangle

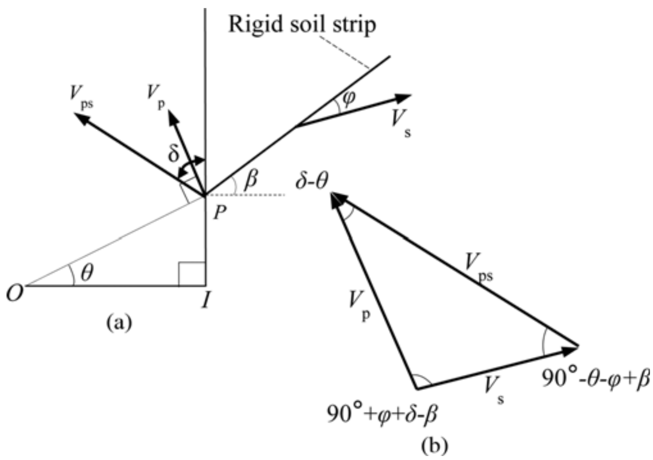

Fig. 6. Relative and Absolute Velocity Vectors for Case $\theta < \delta$: (a) Instantaneous Velocity of Point p and Adjacent Soil Strips, (b) Velocity Vector Triangle

$$V_p = \frac{B\omega}{\cos\theta}. \tag{2}$$

For $\theta > \delta$, according to the velocity compatibility principle and Fig. 5, we can obtain

$$V_s = \frac{V_p \sin(\theta - \delta)}{\cos(\beta - \varphi - \delta)}. \tag{3}$$

For $\theta < \delta$, according to the velocity compatibility principle and Fig. 6, we can also obtain Eq. (3)

Substituting Eq. (2) into Eq. (3)

$$V_s = \frac{B\omega \sin(\theta - \delta)}{\cos(\beta - \varphi - \delta)\cos\theta}. \tag{4}$$

2.3 The Rate of Work Produced by Gravity

The rate of work done by the wall gravity is the vertical component of the velocities multiplied by the weight of the wall, which can be expressed by

$$\dot{W}_{wg} = \gamma_c \omega \left(\frac{1}{2} B^2 H - \frac{1}{6} \mathrm{H}^3 \cot^2 \alpha \right). \tag{5}$$

The rate of work done by each rigid soil strip is the vertical component of the corresponding velocity of each rigid soil strip multiplied by the weight of each rigid soil strip. So, the rate of work done by the total soil wedge can be written as

$$\dot{W}_{sg} = \int_A \gamma_s V_s \sin(\beta - \varphi)\, dA. \tag{6}$$

Substituting Eqs. (1) and (4) into Eq. (6), the Eq. (6) can be rewritten as

$$\begin{aligned} \dot{W}_{sg} &= \int_A \gamma_s V_s \sin(\beta - \varphi)\, dA \\ &= \int_0^{\arctan\left(\frac{H}{B}\right)} \gamma_s V_s \sin(\beta - \varphi) B \cot\beta \sec^2\theta (H - B\tan\theta) \frac{\cos\eta}{\sin\beta - \eta} d\theta \\ &= \frac{\gamma_s \omega f \sin(\beta - \varphi)\cot\beta\cos\eta}{\cos(\beta - \varphi - \delta)\sin\beta - \eta}, \end{aligned} \tag{7}$$

where

$$\begin{aligned} f = &-\frac{1}{48} B^2 \left(\frac{H^2}{B^2} + 1 \right)^{\frac{3}{2}} \left[9H\cos(3\phi - \delta) - 5B\sin(3\phi - \delta) \right] \\ &- 9H\cos(\phi + \delta) + 3B\sin(\phi + \delta) + 3H\cos(\phi - \delta) \\ &- 3H\cos(3\phi + \delta) + 9B\sin(\phi - \delta) + B\sin(3\phi + \delta), \end{aligned} \tag{8}$$

where

$$\phi = \arctan(H/B). \tag{9}$$

2.4 The Rate of Work Produced by Seismic Loads

The pseudo-static method was adopted to evaluate seismic loads, and the directions of the seismic loads were considered the worst-case scenario (see Fig. 2). The rate of work done by the horizontal seismic loads on the wall is the horizontal component of the velocities multiplied by the horizontal seismic load of the wall, which can be expressed by

$$\dot{W}_{ec} = k_h \gamma_c \omega \left(\frac{1}{2} BH^2 - \frac{1}{3} H^3 \cot^2 \alpha \right), \tag{10}$$

where W_{ec} is the rate of work done by the horizontal seismic load on the wall. The rate of work done by each rigid soil strips is the horizontal component corresponding velocity of each rigid soil strips multiplied by the horizontal seismic load on each rigid soil strips. So, the rate of work done by the horizontal seismic load on the soil wedge can be calculated as

$$\dot{W}_{ec} = k_h \gamma_c \omega \left(\frac{1}{2} BH^2 - \frac{1}{3} H^3 \cot^2 \alpha \right), \tag{11}$$

where W_{es} is the rate of work done by the horizontal seismic load on the soil wedge.

Substituting Eqs. (1) and (4) into Eq. (11), we can get

$$\begin{aligned} \dot{W}_{es} &= \int_A k_h \gamma_s V_s \cos(\beta - \varphi)\, dA \\ &= \int_0^{\arctan\left(\frac{H}{B}\right)} k_h \gamma_s V_s \cos(\beta - \varphi) B \cot\beta \sec^2\theta (H - B\tan\theta) \frac{\cos\eta}{\sin\beta - \eta} d\theta \\ &= \frac{k_h \gamma_s \omega f \cos(\beta - \varphi)\cot\beta\cos\eta}{\cos(\beta - \varphi - \delta)\sin\beta - \eta}. \end{aligned} \tag{12}$$

2.5 The Rate of Work Done by Water Pressures Acting on the Wall

In this analysis, considering that the backfill of the wall has a good permeability (k~10^{-3} cm/sec). In other words, water can move freely within the backfill. So, the types of water pressures on the wall include hydrostatic pressures and hydrodynamic pressures. Under seismic conditions, the direction of hydrostatic pressures would not change, while the direction of hydrodynamic pressures would. The directions of the seismic loads are considered the worst-case scenario (see Fig. 2). Ebeling and Morrison (1992) proposed a method for calculating hydrostatic and hydrodynamic pressures, which was also adopted by Choudhury and Ahmad (2007). Solve the hydrostatic pressures on the wall by defining the modified unit weights of water (γ_{we}). So, Hydrostatic pressure on the wall can be expressed as

$$\bar{\gamma}=\frac{h^2}{H^2}\gamma_{sat}+\left(1-\frac{h^2}{H^2}\right)\gamma_d\ , \tag{13}$$

$$\gamma_{we}=\gamma_w+\left(\bar{\gamma}-\gamma_w\right)r_u\ , \tag{14}$$

$$P_{stat}=\frac{1}{2}\gamma_{we}\left(H-h\right)^2\ . \tag{15}$$

And P_{stat} acts at a height of $1/3(H+2h)$ from the base of the wall. Where γ_{we} is the modified unit weights of water; γ_{stat} is the saturated unit weight of the backfill; r_u is defined as the ratio of excess pressure of the initial vertical stress, and $\bar{\gamma}$ is the equivalent unit weight of the soil considering the submergence of the backfill soil. Hydrodynamic pressure (P_{dyn}) acting on the wall back can be expressed

$$P_{dyn}=\frac{7}{12}k_h\gamma_w h^2\ . \tag{16}$$

And P_{dyn} acts at a height of $0.4H+0.6h$ from the base. So, we can get the work done by hydrostatic pressure and hydrodynamic pressure.

$$\dot{W}_{P_{stat}}=\frac{1}{6}\gamma_{we}\left(H-h\right)^2\left(H-2h\right) \tag{17}$$

$$\dot{W}_{P_{dyn}}=\frac{7}{120}\left(2H+3h\right)k_h\gamma_w h^2 \tag{18}$$

2.6 The Rate of Work Produced by Water Pressures on the Soil Wedge

The acting force of the water on the soil wedge includes pore water pressure, excess pore water. As shown in Fig. 7, the distance from the upper surface of the free-body to the ground is Δy, and hydrostatic pressure on the free-body can be expressed as

$$u\left(z\right)=\Delta y\gamma_w\ . \tag{19}$$

Using Ebeling's method (Ebeling and Morrison, 1992), Ebeling expressed the excess pore water pressure in the backfill caused by the earthquake by assuming the ratio of excess pressure of the initial vertical stress (r_u) and still adopted by some scholars Chakraborty and Choudhury (2014a). So, the excess pore water pressure can be expressed by

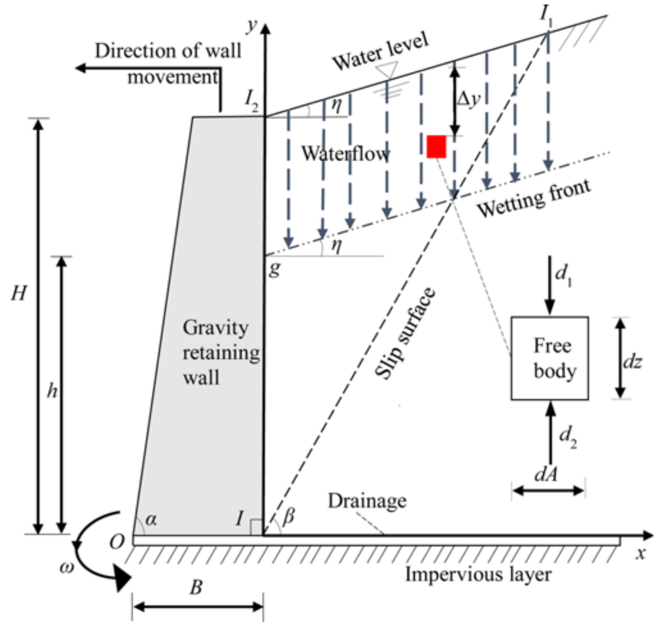

Fig. 7. Water Pressure Acting on the Soil Particle

$$\Delta u\left(z\right)=r_u\sigma_V^{'}\left(z\right)\ . \tag{20}$$

And the initial vertical effective stress can be expressed as

$$\sigma_V^{'}(z)=\Delta y(\gamma_{stat}-\gamma_w)\ . \tag{21}$$

Substituting Eq. (3) into Eq. (2), we can get

$$\Delta u\left(z\right)=r_u\Delta y(\gamma_{stat}-\gamma_w)\ . \tag{22}$$

As shown in Fig. 7, d_1(downward), d_2(upward), and J (seepage force) are water pressures on a free-body respectively:

$$d_1=(1-n)\left[u\left(y\right)+\Delta u\left(y\right)\right]\ , \tag{23}$$

$$d_2=(1-n)\left[u\left(y+dy\right)+\Delta u\left(y+dy\right)\right]\ , \tag{24}$$

$$J=i\gamma_w\ . \tag{25}$$

The water pressure on a free-body can be written as

$$dD=\left(d_2-d_1-J\right)dy\ . \tag{26}$$

As shown in Fig. 8, A completely submerged soil wedge I_2I_1 fg can be divided into numerous "rigid water strips" parallel to the rupture surface II_1, So, we can get the work done by the water on the soil wedge (II_1I_2).

$$\dot{W}_D=\iint V_s\left(d_2\text{-}d_1\text{-}J\right)dydA \tag{27}$$

For $\theta=\theta_1$ (in Fig. 8), the rigid soil strip is partially submerged. So, the area of a rigid water strip can be written as

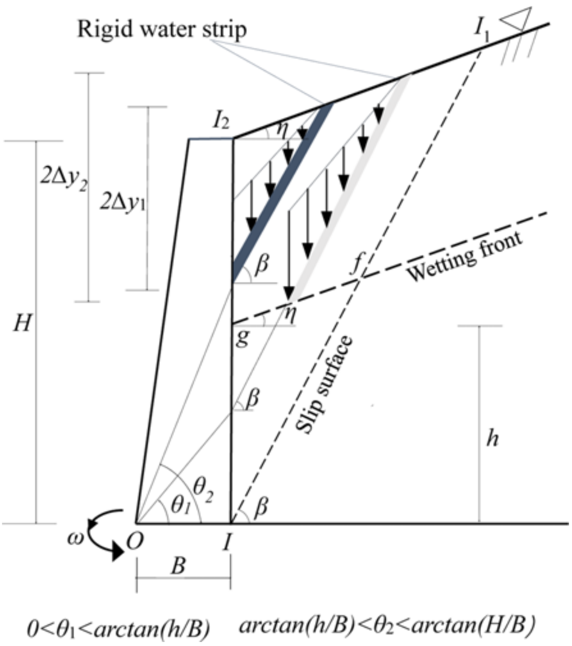

Fig. 8. Water Pressure Distribution

$$dA_2 = (H-h)\cos\beta \frac{\sin(90°+\eta)}{\sin\beta-\eta} dB\tan\theta = B\sec^2\theta(H-h)\cos\beta\frac{\cos\eta}{\sin\beta-\eta}d\theta . \tag{28}$$

For $\theta = \theta_2$ (in Fig. 8), the rigid soil strip is completely submerged. So, the area of a rigid water strip is equal to Eq. (1). Since the water pressure on each rigid soil strip is linearly distributed (in Fig. 8). Therefore, the water pressure on a rigid water strip can be replaced by the water pressure on a free body at the midpoint of the rigid water strip. The midpoint depth of a rigid water strip can be expressed by

$$\Delta y_1 = \frac{(H\text{-}Btan\theta)\cos\eta\sin\beta}{2\cos(\beta-\eta)} , \tag{29}$$

$$\Delta y_2 = \frac{H-h}{2} , \tag{30}$$

Δy_1 is the midpoint depth of a rigid water strip when $\theta = \theta_2$ in Fig. 8, and Δy_2 is the midpoint depth of a rigid water strip when $\theta = \theta_1$ in Fig. 8. We can obtain water pressure D_1 ($\theta = \theta_1$) and D_2 ($\theta = \theta_2$) on the rigid soil strip, respectively:

$$D_1 = R\Delta y_1 - i\gamma_w , \tag{31}$$

$$D_2 = R\Delta y_2 - i\gamma_w , \tag{32}$$

where

$$R = (1-n)\left[\gamma_w + r_u(\gamma_{stat} - \gamma_w)\right] . \tag{33}$$

For $\theta = \theta_2$, the work done by the water pressure on soil wedge can be obtained

$$\begin{aligned}\dot{W}_{D_2} &= \int D_2 V_s dA \\ &= \int_{arctan\frac{h}{B}}^{arctan\frac{H}{B}} \left\{\frac{(H\text{-}Btan\theta)R\cos\eta\sin\beta}{2\cos(\beta-\eta)} - i\gamma_w\right\}\left[B\omega\frac{\sin(\theta-\delta)}{\cos(\beta-\varphi-\delta)\cos\theta}\right] \\ &\quad \left[B\sec^2\theta(H-B\tan\theta)\cos\beta\frac{\cos\eta}{\sin\beta-\eta}\right]d\theta \\ &= \frac{B^2R\omega\cos\eta\cos\eta\sin2\beta}{2\sin2(\beta-\eta)\cos(\beta-\varphi-\delta)}(f_2-f_3) - \frac{B^2\omega\gamma_w i\cos\beta\cos\eta}{\sin\beta-\eta}(f-f_1),\end{aligned} \tag{34}$$

$$\begin{aligned}f_1 = &-\frac{1}{48}B^2\left(\frac{H^2}{B^2}+1\right)^{\frac{3}{2}}\left[9H\cos(3\lambda-\delta)-5B\sin(3\lambda-\delta)\right] - \\ &9H\cos(\lambda+\delta)+3B\sin(\lambda+\delta)+3H\cos(\lambda-\delta) \\ &-3H\cos(3\lambda+\delta)+9B\sin(\lambda-\delta)+B\sin(3\lambda+\delta),\end{aligned} \tag{35}$$

where $\lambda = \arctan(h/B)$

$$\begin{aligned}f_2 = &\,2B^2H\tan\frac{\lambda-\delta}{2}\sin(2\lambda-\delta)+4H^2B\tan^3 2\lambda\sin(\delta) \\ &+8HB\cos(3\delta+\lambda)\tan^5\frac{\lambda}{2}+2H^2B^2\sin(3\delta-\lambda)\tan^4\frac{\lambda}{2} \\ &-\frac{4}{3}H^2\cos\delta - H\tan\frac{\lambda}{2}(2B\sin\delta+H\sin\delta) \\ &+2HB\tan^4\frac{\lambda}{2}\sin\delta\left(H\cos(\delta+\lambda)+2H\sin\delta\right)+ar\tan\left(\sin\frac{\lambda}{2}\right) \\ &\left(H\cos(\delta+\lambda)+B^2\cos(\delta+4\lambda)\right),\end{aligned} \tag{36}$$

$$\begin{aligned}f_3 = &\,2B^2H\tan\frac{\eta-\delta}{2}\sin(2\eta-\delta)+4H^2B\tan^3 2\eta \\ &+8HB\cos(3\delta+\eta)\tan^5\frac{\lambda}{2}+2H^2B^2\sin(3\delta-\eta)\tan^4\frac{\eta}{2}-\frac{4}{3}H^2\cos\delta \\ &-H\tan\frac{\eta}{2}(2B\sin\delta+H\sin\delta)+2HB\tan^4\frac{\eta}{2}\left(H\cos(\delta+\eta)+2H\sin\delta\right) \\ &+ar\tan\left(\sin\frac{\eta}{2}\right)\left(H\cos(\delta+\eta)+B^2\cos(\delta+4\eta)\right)\cdot\end{aligned} \tag{37}$$

For $\theta = \theta_1$, the work done by the water pressure on soil wedge can be obtained

$$\begin{aligned}\dot{W}_{D_1} &= \int D_1 V_s dA_1 \\ &= \int_0^{arctan\frac{h}{B}}\left[\frac{\sin(\theta-\delta)B\omega}{\cos(\beta-\varphi-\delta)\cos\theta}\right]\left\{\frac{R(H-h)}{2}-i\gamma_w\right\}\left[\frac{B\sec^2\theta(H-h)\cos\eta\cos\beta}{\sin\beta-\eta}\right]d\theta \\ &= \frac{B^2\omega\sin\delta\cos\beta(\cos\delta-\sin2\lambda)(RH-Rh-2i\gamma_w)\cos\eta(H-h)}{2(\cos2\lambda+1)\cos(\beta-\varphi-\delta)\sin(\beta-\eta)} .\end{aligned} \tag{38}$$

Since the backfill is cohesionless, the rate of energy dissipation is zero. Therefore, the energy balance can be obtained as

$$\dot{W}_{es} + \dot{W}_{ec} + \dot{W}_{sg} + \dot{W}_{wg} + \dot{W}_{D} + \dot{W}_{P_{stat}} + \dot{W}_{dyn} = 0 . \tag{39}$$

Substituting Eqs. (5), (6), (7), (10), (12), (17), (18), (27) into Eq. (39) and we can get k_h

$$k_h = \frac{\gamma_c\left(\frac{1}{2}B^2H - \frac{1}{6}H^3\cot^2\alpha\right) - \frac{\gamma_s f\sin(\beta-\varphi)\cot\beta\cos\eta}{\cos(\beta-\varphi-\delta)\sin(\beta-\eta)} - \frac{1}{6}\gamma_{we}(H-h)^2(H+2h) - f_4}{\gamma_c\left(\frac{1}{2}BH^2 - \frac{1}{3}H^3\cot^2\alpha\right) + \frac{\gamma_s f\cos(\beta-\varphi)\cot\beta\cos\eta}{\cos(\beta-\varphi-\delta)\sin(\beta-\eta)} + \frac{7}{60}\gamma_w h^2(2H+3h)} . \tag{40}$$

The critical seismic coefficient k_{cr} is obtained by minimizing

k_h with respect to β. This means that Eq. (40) satisfies $(\partial k_h/\partial\beta)=0$, we can get an analytic solution for the critical value of β_{cr}, and substitute the critical value of β_{cr} into the original equation. We can obtain the threshold of seismic yield acceleration coefficient k_{cr}. But the analytic solution of β_{cr} is too complicated, this paper uses numerical methods to solve k_{cr}

3. Calculation Examples and Parameter Analysis

3.1 The Effect of h on k_{cr}

Calculated parameters: $H = 5$ m; $\gamma_w = 10$ kN/m^3; $\gamma_c = 24$ kN/m^3; $w = 30\%$; $\gamma_s = 16$ kN/m^3; $\gamma_{stat} = 19$ kN/m^3; $r_u = 0.2$; $n = 0.3$; $B = 2.2$ m; $i = 0.5$; $\eta = 5°$; $\delta = 15°$; $\alpha = 80°$; $\varphi = 40°, 45°$.

As shown in Fig. 9, the infiltration depth of rainwater (H-h) has a significant effect on yield acceleration coefficient k_{cr}, and yield acceleration coefficient k_{cr} decrease from 0.3243 to 0.0794 when the value of infiltration depth of rainwater (H-h) increased from 1m to 4 m.

3.2 The Effect of η on k_{cr}

Calculated parameters: $H = 5$ m; $\gamma_w = 10$ kN/m^3; $\gamma_c = 24$ kN/m^3;

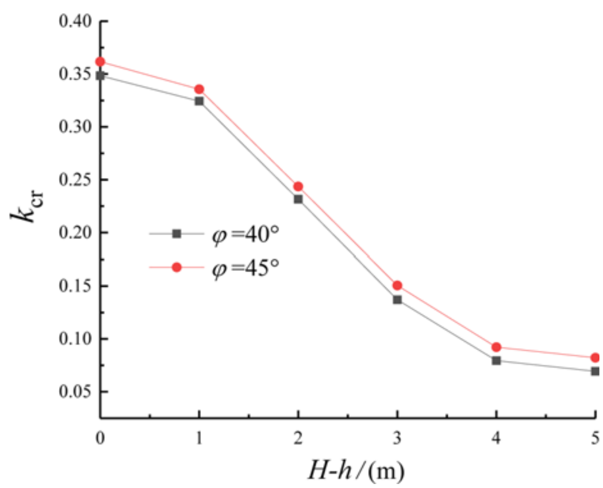

Fig. 9. Effect of Infiltration Depth of Rainwater H-h on k_{cr}

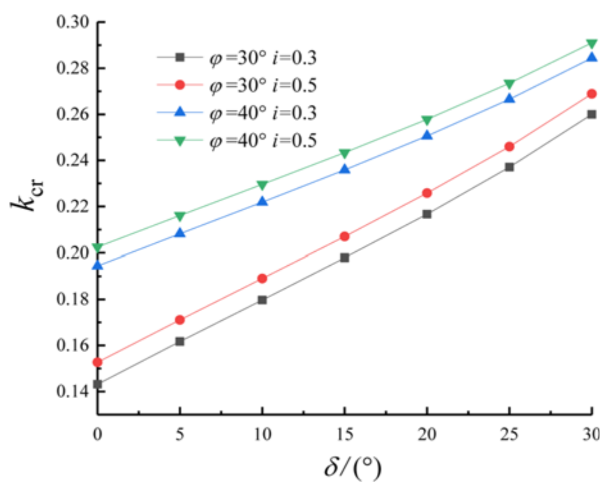

Fig. 10. Effect of Wall-Soil Friction Angle δ on k_{cr}

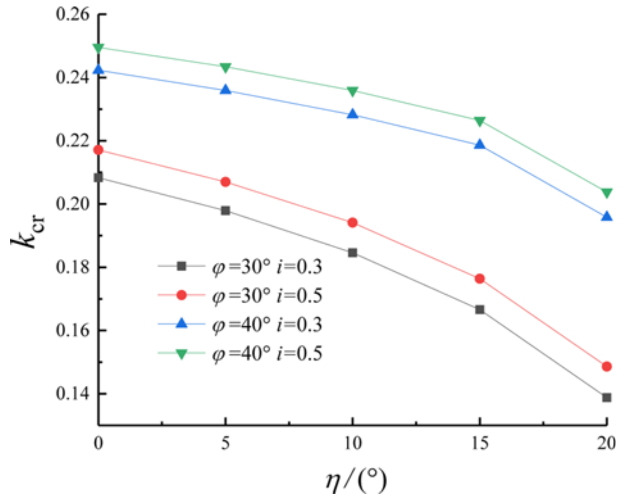

Fig. 11. Effect of the Backfill Inclination η on k_{cr}

$w = 30\%$; $\gamma_s = 16$ kN/m^3; $\gamma_{stat} = 19$ kN/m^3; $r_u = 0.2$; $n = 0.3$; $B = 1.8$ m; $\eta = 5°$; $\alpha = 80°$; $i = 0.3, 0.5$; $\varphi = 30°, 40°$.

Figure 10 shows that the value of yield acceleration coefficient k_{cr} increases with an increase in the value of wall-soil friction angle δ and hydraulic gradient i. It is worth noting that k_{cr} is more susceptible to φ than k_{cr} to i. This means that increasing internal friction angle φ would be a wise choice to improve the overturning resistance of the gravity retaining wall in the seismic design.

3.3 The Effect of η on k_{cr}

Calculated parameters: $H = 5$ m; $\gamma_w = 10$ kN/m^3; $\gamma_c = 24$ kN/m^3; $w = 30\%$; $\gamma_s = 16$ kN/m^3; $\gamma_{stat} = 19$ kN/m^3; $r_u = 0.2$; $n = 0.3$; $B = 1.8$ m; $\delta = 15°$; $\alpha = 80°$; $i = 0.3, 0.5$; $\varphi = 30°, 40°$.

Figure 11 shows that with an increase in the value of the backfill inclination η, the yield acceleration coefficient will reduce. When the value of the backfill inclination η exceeds 15°, the seismic yield acceleration coefficient will decrease rapidly.

4. Comparison of Results

In order to verify the accuracy of the calculation model, a numerical model is established by ABAQUS (in Fig. 12).

Figure 12 shows a retaining wall with a height 5 m, thickness 2 m, width 2.2 m, and the wall front inclination $\alpha = 80°$. To ensure that the boundary of the section does not significantly affect the results, the length of backfill is 12 m. The backfill is sandy soil which other parameters involved in the analysis are: $\gamma_w = 10$ kN/m^3; $w = 30\%$; $\gamma_s = 16$ kN/m^3, $\varphi = 40°$, $n = 0.3$; $\eta = 10°$. A surface-to-surface contact form is established between the retaining wall and the backfill. The tangential contact between the retaining wall and the backfill is Penalty and the coefficient of friction is 0.3. While the normal contact between the backfill and the retaining wall is Hard. The retaining wall is defined as an elastic material and the backfill is a molar coulomb material. The surface on both sides of the soil is constrained by normal

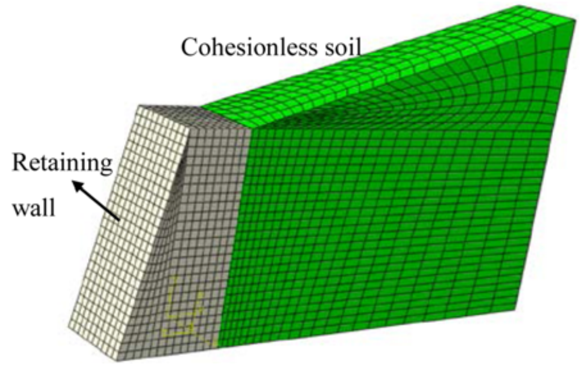

Fig. 12. Numerical Model by Abaqus

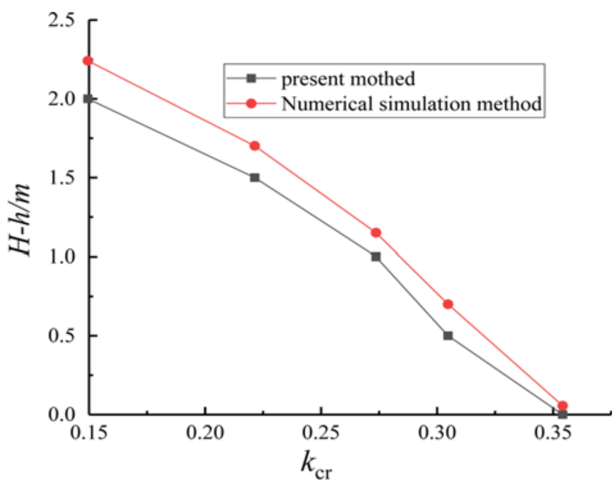

Fig. 13. The Relationship between k_{cr} and Infiltration Depth *H-h*

direction, the lower bottom is constrained by both tangential and normal directions and the wall is restrained so that it can only rotate around the toe of the wall. We selected the value of the horizontal seismic coefficient to simulate the rainfall infiltration. Then the maximum infiltration depth of rainwater was compared with the theoretical formula Eq. (40), we can get Fig. 13.

As can be seen from Fig. 13, although the rainfall infiltration depth obtained by numerical simulation is less than that obtained by theoretical analysis, there is still a good agreement. In the process of numerical simulation, different meshing methods will lead to different results. Therefore, five different mesh densities were used to analyze the mesh sensitivity of the retaining wall model. For $k_h = 0.2$, we can get the maximum infiltration depth of rainwater in Table 1.

From Table 1, we can see that the retaining wall model is not sensitive to meshing.

Table 1. Five Different Unit Numbers

	Mesh1	Mesh2	Mesh3	Mesh4	Mesh5
Number of units	450	680	1,140	1,830	2,750
Maximum infiltration depth	1.4900	1.4970	1.4940	1.4932	1.4942

5. Conclusions

1. A rainwater infiltration model is introduced for analyzing the characteristics of rainwater infiltration. A formula to calculate seismic yield acceleration under coupling conditions of earthquakes and rainfall is deduced by the upper-bound limit method.
2. The establishment of a numerical analysis model using finite element software (Abaqus) has verified the accuracy of the results in this paper.
3. Results analysis revealed a large effect size of infiltration depth of rainwater and the backfill inclination on the seismic yield acceleration coefficient. When the infiltration depth of rainwater exceeds one-fifth of the height of the retaining wall and the backfill inclination exceeds 15°, the seismic rotational stability of the gravity retaining wall will decrease significantly.

Acknowledgments

Not Applicable

Nomenclature

B = Width of the wall
dA_1 = Area of a rigid water strip when $\theta = \theta_2$ in Fig. 8
dA_2 = Area of a rigid water strip when $\theta = \theta_1$ in Fig. 8
H = Height of the wall
h = Height of the point g in Fig. 2
i = Hydraulic gradient
J = Seepage force
k_{cr} = Yield acceleration coefficient
k_h = Horizontal seismic yield acceleration coefficient
n = The porosity of soil mass
O = Toe of the wall
P_{dyn} = Hydrodynamic pressure on the wall
P_{stat} = Hydrostatic pressure on the wall
r_u = Pore water pressure ratio
V_p = Velocity of point P in Figs. 5 and 6
V_{ps} = Relative velocity between V_s and V_p
V_s = Velocities of the rigid adjacent to point P in Figs. 5 and 6
$\dot{W}_{cg}$ = Rate of work done by the soil wedge
$\dot{W}_{D}$ = Rate of work done by water on soil wedge
$\dot{W}_{D1}$ = The work done by the water pressure on soil wedge when $\theta = \theta_1$ in Fig. 8
$\dot{W}_{D2}$ = The work done by the water pressure on soil wedge when $\theta = \theta_2$ in Fig. 8
$\dot{W}_{dyn}$ = Rate of work done by hydrostatic pressure on the wall
$\dot{W}_{ec}$ = Rate of work done by horizontal inertial force of the wall
$\dot{W}_{es}$ = Rate of work done by horizontal inertial force of soil wedge
$\dot{W}_{stat}$ = Rate of work done by hydrodynamic pressure

$\dot{W}_{wg}$ = Rate of work done by the wall weight
w = Backfill moisture content
Δy_1 = The midpoint depth of a rigid water strip when $\theta = \theta_1$ in Fig. 8
Δy_2 = The midpoint depth of a rigid water strip when $\theta = \theta_2$ in Fig. 8
$\Delta u(z)$ = Excess pore water pressure
α = The wall front inclination
β = Inclination angle of rupture
β_{cr} = β corresponding to k_{cr}
$\bar{\gamma}$ = Equivalent unit weight of the soil
γ_c = Unit weight of the retaining wall
γ_d = Unit weight of dry soil
γ_s = Unit weight of soil
γ_{stat} = Saturated unit weight of soil
γ_w = Unit weight of water
γ_{we} = The modified unit weights of water
δ = Wall-soil friction angle
η = The backfill inclination
λ = Arctan (h/B)
θ = Inclination angle of line OP in Fig. 3
$\sigma_v'(z)$ = The initial vertical effective stress
ϕ = Arctan (H/B)
φ = Internal friction angle
ω = Angular velocity of the wall about toe

ORCID

Xiaoguang Li https://orcid.org/0000-0003-0639-8331

References

Ahmad SM, Choudhury D (2010) Seismic rotational stability of waterfront retaining wall using pseudodynamic method. *International Journal of Geomechanics* 10(1):45-52, DOI: 10.1061/(ASCE)1532-3641(2010)10:1(45)

Augusto Filho O, Fernandes MA (2019) Landslide analysis of unsaturated soil slopes based on rainfall and matric suction data. *Bulletin of Engineering Geology and the Environment* 78(6):4167-4185, DOI: 10.1007/s10064-018-1392-5

Bo A, Chun Z, Kuiming L, Sitong L, Zhigang T, Haipeng L, Haoran Y (2019) The influence of rainfall on landslide stability of an open-pit mine: The case of Haizhou open-pit mine. *Geotechnical and Geological Engineering* 37(4):3367-3378, DOI: 10.1007/s10706-019-00851-y

Capparelli G, Damiano E, Greco R, Olivares L, Spolverino G (2020) Physical modeling investigation of rainfall infiltration in steep layered volcanoclastic slopes. *Journal of Hydrology* 580:124199, DOI: 10.1016/j.jhydrol.2019.124199

Chakraborty D, Choudhury D (2014a) Sliding stability of non-vertical waterfront retaining wall supporting inclined backfill subjected to pseudo-dynamic earthquake forces. *Applied Ocean Research* 47:174-182, DOI: 10.1016/j.apor.2014.05.004

Chakraborty D, Choudhury D (2014b) Stability of non-vertical waterfront retaining wall supporting inclined backfill under earthquake and tsunami. *Ocean Engineering* 78:1-10, DOI: 10.1016/j.oceaneng.2013.11.024

Chandrasekaran SS, Sayed Owaise R, Ashwin S, Jain RM, Prasanth S, Venugopalan RB (2013) Investigation on infrastructural damages by rainfall-induced landslides during November 2009 in Nilgiris, India. *Natural Hazards* 65(3):1535-1557, DOI: 10.1007/s11069-012-0432-x

Chen WF, Liu XL (1990) Limit analysis in soil mechanics. Elsevier, Amsterdam, The Netherlands

Choudhury D, Ahmad SM (2007) Stability of waterfront retaining wall subjected to pseudo-static earthquake forces. *Ocean Engineering* 34(14-15):1947-1954, DOI: 10.1016/j.oceaneng.2007.03.005

Drucker DC, Prager W, Greenberg HJ (1952) Extended limit design theorems for continuous media. *Quarterly of Applied Mathematics* 9(4):381-389, DOI: 10.1090/qam/45573

Ebeling RM, Morrison EE (1992) The seismic design of waterfront retaining structures. US Army Corps of Engineers, Washington DC, USA

Green WH, Ampt GA (1911) Studies of soil physics, Part I – The flow of air and water through soils. *Journal of Agricultual Science* 4:1-24, DOI: 10.1017/S0021859600001441

Huang D, Liu J (2016) Upper-bound limit analysis on seismic rotational stability of retaining wall. *KSCE Journal of Civil Engineering* 20(11):2664-2669, DOI: 10.1007/s12205-016-0471-z

Iverson RM (2000) Landslide triggering by rain infiltration. *Water Resources Research* 36(7):1897-1910, DOI: 10.1029/2000WR900090

Jo S-B, Ha J-G, Lee J-S, Kim D-S (2017) Evaluation of the seismic earth pressure for inverted T-shape stiff retaining wall in cohesionless soils via dynamic centrifuge. *Soil Dynamics and Earthquake Engineering* 92:345-357, DOI: 10.1016/j.soildyn.2016.10.009

Leshchinsky D, Ebrahimi S, Vahedifard F, Zhu F (2012) Extension of Mononobe–Okabe approach to unstable slopes. *Soils and Foundations* 52(2):239-256, DOI: 10.1016/j.sandf.2012.02.004

Li X, Su L, Wu Y, He S (2015) Seismic stability of gravity retaining walls under combined horizontal and vertical accelerations. *Geotechnical and Geological Engineering* 33(1):161-166, DOI: 10.1007/s10706-014-9815-y

Li X, Wu Y, He S (2010) Seismic stability analysis of gravity retaining walls. *Soil Dynamics and Earthquake Engineering* 30(10):875-878, DOI: 10.1016/j.soildyn.2010.04.005

Mononobe N, Matsuo H (1929) On the determination of earth pressure during earthquake. Proceedings of the World Engineering Conference, 177-185

Okabe S (1924) General theory on earth pressure and seismic stability of retaining wall and dam. *Journal of Japan Society of Civil Engineers* 10(6):1277-1323

Pain A, Choudhury D, Bhattacharyya SK (2017) Seismic rotational stability of gravity retaining walls by modified pseudo-dynamic method. *Soil Dynamics and Earthquake Engineering* 94:244-253, DOI: 10.1016/j.soildyn.2017.01.016

Ren F, Huang Q, Wang G (2020) Shaking table tests on reinforced soil retaining walls subjected to the combined effects of rainfall and earthquakes. *Engineering Geology* 267:105475, DOI: 10.1016/j.enggeo.2020.105475

Song J, Fan Q, Feng T, Chen Z, Chen J, Gao Y (2019) A multi-block sliding approach to calculate the permanent seismic displacement of slopes. *Engineering Geology* 255:48-58, DOI: 10.1016/j.enggeo.2019.04.012

Wilson P, Elgamal A (2015) Shake table lateral earth pressure testing with dense c-ϕ backfill. *Soil Dynamics and Earthquake Engineering* 71:13-26, DOI: 10.1016/j.soildyn.2014.12.009

Xie M, Esaki T, Cai M (2004) A time-space based approach for mapping rainfall-induced shallow landslide hazard. *Environmental Geology* 46(6-7):840-850, DOI: 10.1007/s00254-004-1069-1

Yeh P-T, Lee KZ-Z, Chang K-T (2020) 3D effects of permeability and strength anisotropy on the stability of weakly cemented rock slopes subjected to rainfall infiltration. *Engineering Geology* 266:105459, DOI: 10.1016/j.enggeo.2019.105459

Zeng X, Steedman RS (2000) Rotating block method for seismic displacement of gravity walls. *Journal of Geotechnical and Geoenvironmental Engineering* 126(8):709-717, DOI: 10.1061/(ASCE)1090-0241(2000)126:8(709)

Zhang C, Chen X, Fan W (2016) Overturning stability of a rigid retaining wall for foundation pits in unsaturated soils. *International Journal of Geomechanics* 16(4), DOI: 10.1061/(ASCE)GM.1943-5622.0000613

Zhang G, Qian Y, Wang Z, Zhao B (2014) Analysis of rainfall infiltration law in unsaturated soil slope. *The Scientific World Journal* 2014:1-7, DOI: 10.1155/2014/567250